Damage and fracture behaviours in advanced heat resistant materials during slow strain rate test at high temperature

Mattias Calmunger[1,*], Guocai Chai[1, 2], Sten Johansson[1], Johan Moverare[1]

[1] Division of Engineering Materials, Department of Management and Engineering, Linköping University, SE-58183 Linköping, Sweden
[2] AB Sandvik Material Technology R&D center, SE-81181 Sandviken, Sweden
* Corresponding author: mattias.calmunger@liu.se

Abstract As a renewable energy resource, biomass or biomass co-firing in coal-fired power plants with high efficiency are desired which corresponding to elevated temperature and high pressure. An upgrade of the material performance to austenitic stainless steels is therefore required in order to meet the increased demands due to the higher temperature and the more corrosive environment. These materials suffer from creep and fatigue damage during the service. In this study, these behaviours are evaluated using slow strain rate testing (SSRT) with strain rate down to $1*10^{-6}$/s at temperature up to 700°C. The influence of temperature and strain rate on strength and ductility in one austenitic stainless steel and one nickel base alloys are investigated. The damage and fracture due to the interaction between moving dislocations and precipitates are studied using electron channelling contrast imaging (ECCI) and electron backscattering diffraction (EBSD). The deformation and damage mechanisms active during SSRT are essentially the same as under creep. The influence of dynamic strain ageing (DSA) phenomena that appears in the tested temperature and strain rate regime is also discussed, DSA is intensified by increased temperature and decreased strain rate.

Keywords Elevated temperature, slow strain rate, biomass power plant, austenitic stainless steel, nickel base alloy.

1. Introduction

Biomass or biomass co-firing in coal-fired power plants is a contribution to renewable energy resources for sustainable energy production. Also high efficiency which requires higher temperature and pressure is highly desired. However, the materials used in those power plants with increasing temperature and pressure also need to be resistant to the corrosive atmosphere connected to combustion of biomass fuel [1, 2].

In the operating temperature range of biomass or biomass co-firing coal-fired power plants, austenitic materials often show dynamic strain ageing (DSA). The temperature regime of DSA is from 200 to 800°C for austenitic materials [3, 4] and arises during plastic deformation from interaction between solute atoms related to bulk or pipe diffusion and mobile dislocations or forest junctions[5, 6]. Temperature and strain rate directly influence diffusing solute atoms and the mobility of dislocations respectively, which effects DSA [6]. At elevated temperatures (400°C to 650°C) nitrogen and/or substitutional chromium atoms are responsible for DSA [7, 8]. Portevin-Le Châtelier (PLC) effect which is serrated yielding in the stress-strain curve, characterizes DSA. The PLC effect is due to the pinning and unpinning of dislocations or formation of new dislocations [9].

These materials can undertake low deformation rate from 10^{-5}/s (low cycle fatigue) to 10^{-7}/s (creep) during service. This study was focused on damage and fracture mechanisms related to low strain rate and high-temperature in two austenitic materials. Using uniaxial slow strain rate tensile testing (SSRT) at high-temperatures, the influence of low strain rates on these mechanisms could be investigated. Also precipitation due to high-temperature and deformation could be coupled to the damage and fracture behaviour.

2. Materials and experimental details

2.1. Materials

The austenitic stainless steels, AISI 316L and the nickel-base alloys, Alloy 617 were used in this study. Both types were solution treated before testing. Table 1 shows the chemical composition of the materials.

Table 1. Nominal composition of the investigated materials in wt%.

Material	C	Si	Mn	Cr	Ni	W	Co	Cu	Nb	N	Mo	Fe
AISI 316L	0.04	0.4	1.7	17	12	-	-	-	-	-	2.6	Bal.
Alloy 617	0.1	-	-	22.5	53.8	-	12	-	-	0.5	9	1.1

2.2. Tensile deformation

For the slow strain rate tensile testing (SSRT) a Roell-Korthaus and an Instron 5982 tensile test machines were employed. The tensile test machines were equipped with a MTS 653 furnace and Magtec PMA-12/2/VV7-1 extensometer and ElectroHeat Sweden furnace and Epsilon extensometer respectively, both active in air environments. Round-bar specimens with 5 mm in diameter and 50 mm gauge length were used. The tensile tests were carried out at a strain rate of $2*10^{-3}s^{-1}$ down to $10^{-6}s^{-1}$. Three temperatures: room temperature (RT), 650°C and 700°C, were used. Alloy 617 was tested using strain rates $10^{-2}s^{-1}$, $2*10^{-3}s^{-1}$, $10^{-3}s^{-1}$, $10^{-4}s^{-1}$, $10^{-5}s^{-1}$ and $10^{-6}s^{-1}$, AISI 316L was tested using strain rates $2*10^{-3}s^{-1}$ and $10^{-6}s^{-1}$.

2.3. Scanning electron microscopy investigation

For the microstructural investigation of deformation and fracture behaviour the scanning electron microscopy (SEM) techniques electron channeling contrast imaging (ECCI) and electron backscatter diffraction (EBSD) were used. ECCI uses the interaction between backscattered electrons and the crystal planes to generate contrast resulting in an image where local orientation, defects and strain fields are shown as contrast variations [10].

3. Results

3.1. Strain rate and temperature influence on tensile deformation and damage

Low strain rates and elevated temperatures are increasing the probability of dynamic strain ageing (DSA), because the diffusion rate of the solute atoms increases and rate of dislocation movement decreases. During DSA the deformation mechanisms is shifting towards planar deformation [7]. None of the tested materials showed DSA at room temperature, but both materials showed DSA at elevated temperatures for all tested strain rates. For a strain rate of 10^{-6}/s at both elevated temperatures, AISI 316L and Alloy 617 show different types of PLC effects. AISI 316L display B-type and Alloy 617 shows C-type serrated yielding, see fig.1. B-type serrations means that the stress oscillates from a origin stress level and C-type of serration is characterized by a sudden drop in stress and then raises to the normal stress level [8, 9]. Alloy 617 show serrated yielding from low strain values until fracture for all tested strain rates at both elevated temperature except of strain rates 10^{-3}/s and 10^{-4}/s. At both elevated temperatures and strain rate 10^{-3}/s serrated yielding is present at low strain levels up to around 20% but DSA also appears just before fracture, see fig. 1a). For 10^{-4}/s at 650°C serrated yielding disappears after approximately 4% strain and after around 12%

with a few serration drops at 22% strain at 700°C. At room temperature the elongation to fracture increases with decreasing strain rate for AISI 316L, at a strain rate of $2*10^{-3}$/s it is 53% and 66% at 10^{-6}/s, see fig.1b). This behaviour is due to the lower deformation rate that causes the dislocation mobility to decrease and therefore resulting in a lower stress level when using a strain rate of 10^{-6}/s. At elevated temperatures and low strain rates AISI 316L show a decrease in the stress-level during tensile tests due to recovery that could be related to recovery-creep [11], see fig.1b), also features related to dynamic recrystallization can be found in the microstructure (fig.4) [12].

The strain rate influences the ductile response of Alloy 617, as shown in fig. 2 a). From 10^{-2}/s to 10^{-3}/s the ductility increases at both temperatures and continues to increase for strain rates of 10^{-4}/s at 650°C but decrease slightly at 700°C. With even slower strain rates the ductility decreases even more for both temperatures, 700°C have lower ductility than 650°C at a strain rate of 10^{-6}/s but have a higher tensile stress which can explain the differences in ductility. Alloy 617 has much higher ductility (A_{RT}=70.5%) and tensile stress (Rm_{RT}=709MPa) when it is deformed at room temperature than at elevated temperature ($A_{700°C}$=10.3% and $Rm_{700°C}$=489MPa) when using a strain of rate 10^{-6}/s, see fig.2. This behaviour is most likely due to grain boundary embrittlement coused by chromium rich precipitation in the grain boundaries, shown in fig.6.

In the DSA regime nano-twins can show up as a deformation mechanism [13]. AISI 316L material showed nano-twins close to the surface of the specimen. Other deformation mechanism in the microstructure of the SSRT tested samples was slip bands (SB) and planar slip. Fig.3 displays probable future damage due to interaction between slip bands and precipitates (fig.3 b)) and nano-twins and precipitates. Contrast differences that could be related to stress concentrations spots which is or will be future damage can be observed where these interactions appear in fig. 3 b) and c).

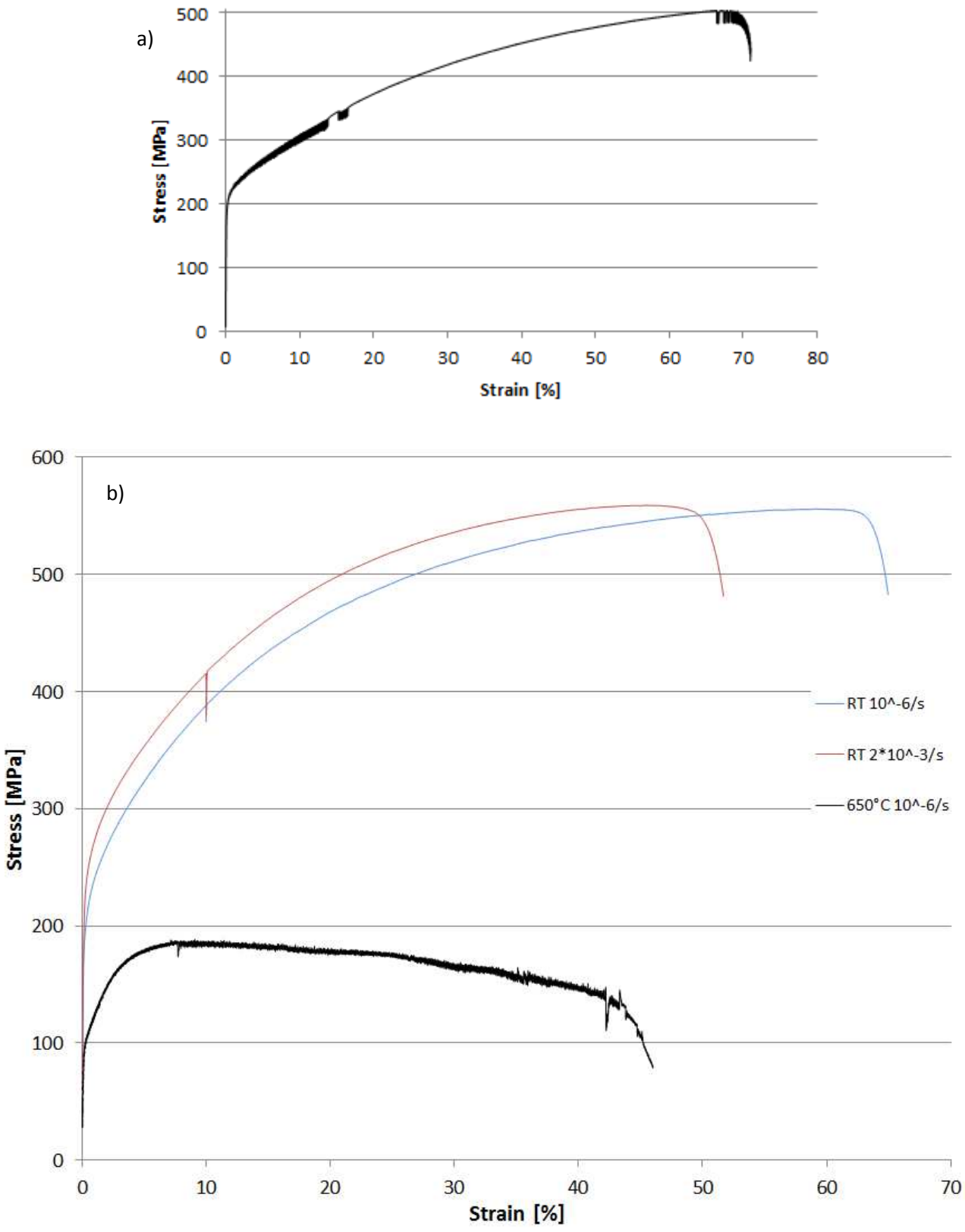

Figure 1. Engineering stress-strain curves showing a) C-type serration in Alloy 617 tensile tested at 700°C using strain rate 10^{-3}/s and b) B-serration in AISI 316L tensile tested at 650°C using strain rate 10^{-6}/s (black curve) and two curves showing AISI 316L tested at room temperature (RT) using strain rates 10^{-6}/s and $2*10^{-3}$/s (blue and red curve respectively).

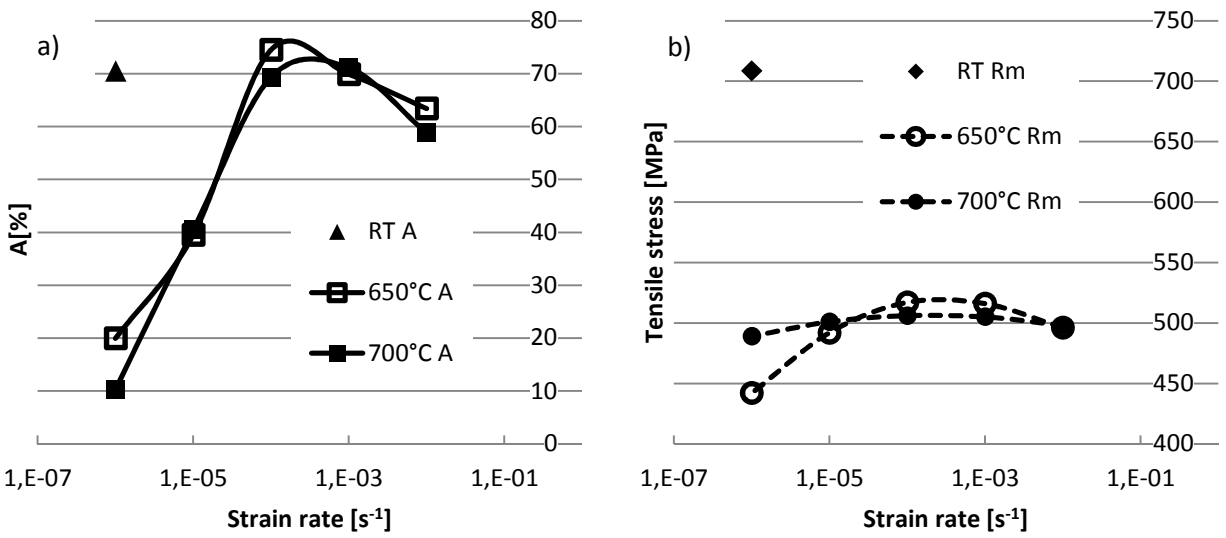

Figure 2. Influence of a) strain rate on ductility (A) and b) tensile stress (R_m) levels for Alloy 617.

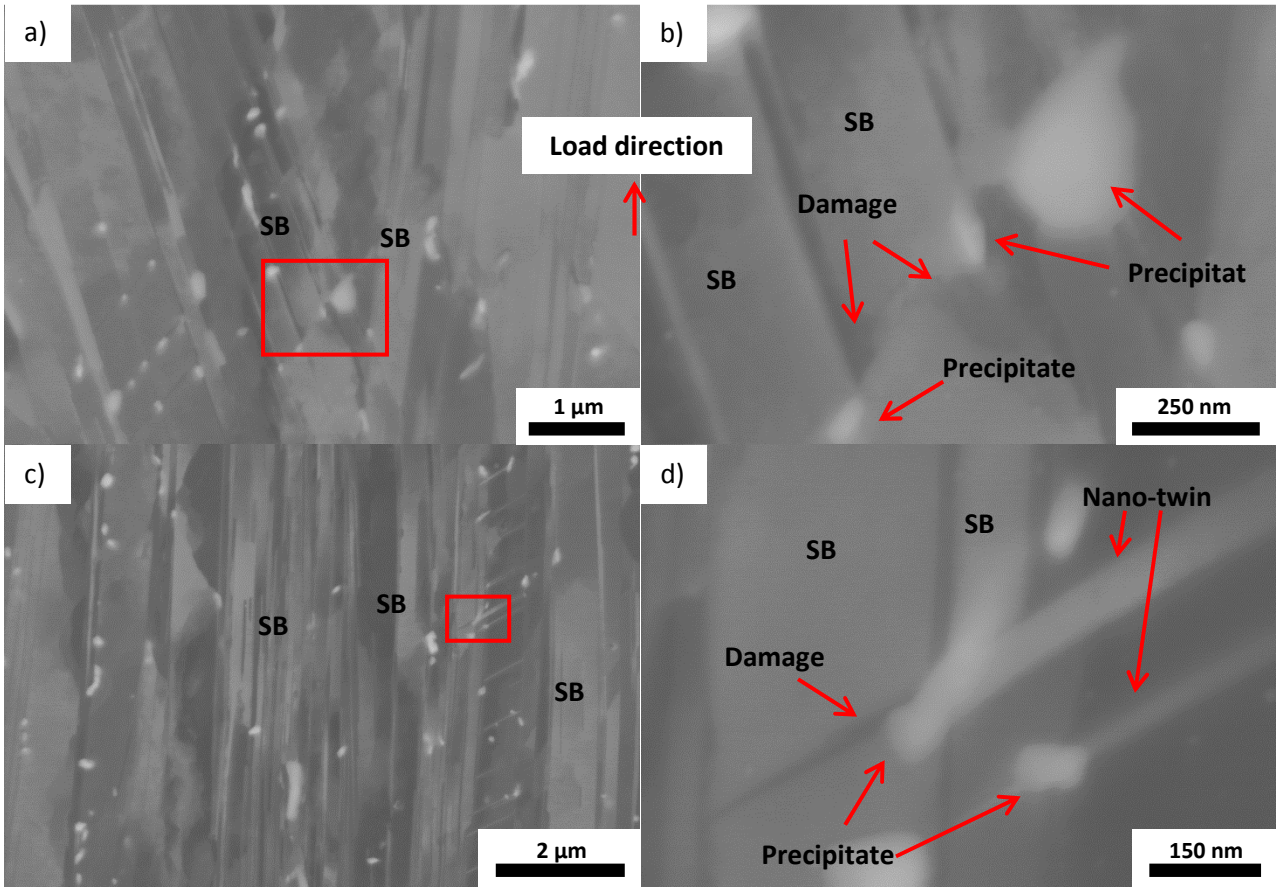

Figure 3. ECCI imaging of AISI 316L deformed to 46% strain, at a strain rate of 10^{-6}/s and 700°C, a) slip bands (SB) with two different directions interacting with precipitates, b) magnification of damage or probable future damage due to interaction between precipitate and slip bands, c) other location with slip bands and nano-twins interacting with precipitates and d) magnification of damage or probable future damage due to interaction between slip bands, nano-twins and precipitate. It is the same load direction in all the pictures.

Other damage behaviour in AISI 316L is shown in fig.4. At room temperature the deformation and damage behaviour is similar for strain rates of $2*10^{-3}$/s and 10^{-6}/s. Common damage appearing away from fracture zone is slip bands creating voids when intersecting with each other, grain boundaries or precipitates. Voids due to intersection between slip bands and grain boundaries, around 15mm away from the fracture surface are displayed in fig. 4 a). Voids also occur due to heavy deformation from shear bands as in fig.4 b). Near the fracture surface the microstructure is heavily deformed from multi-direction slip bands, shear bands and planar slip. Deformation bands with features looking like subcells appear near the fracture surface at room temperature for strain rates of $2*10^{-3}$/ and 10^{-6}/s. At elevated temperature the deformation bands look recrystallized as can be seen in fig. 4 c) and d). The EBSD analysis in fig.5 reveals that the areas that look like recrystallization has taken place (see fig.5 a)) don't show any new grains in AISI 316L at 650°C and a strain rate of 10^{-3}/s. Fig.5 b) shows the local misorientation in gray scale together with inversed pole figure (IPF) in color scale, and the brighter patterns correspond to local misorientation values above 4° and up to 5°. These brighter patterns have good correlation to some of the subcell or grains that can be seen in fig.5 a). The crystallographic orientation differs but doesn't give clear distinction between the supposed subcells or grains and the matrix and thus no evidence of recrystallization is found. The analysis in fig.5 is made in mostly one single grain or annealing twin, showing precipitates in the grain boundaries as white zero-solution in fig.5 b).

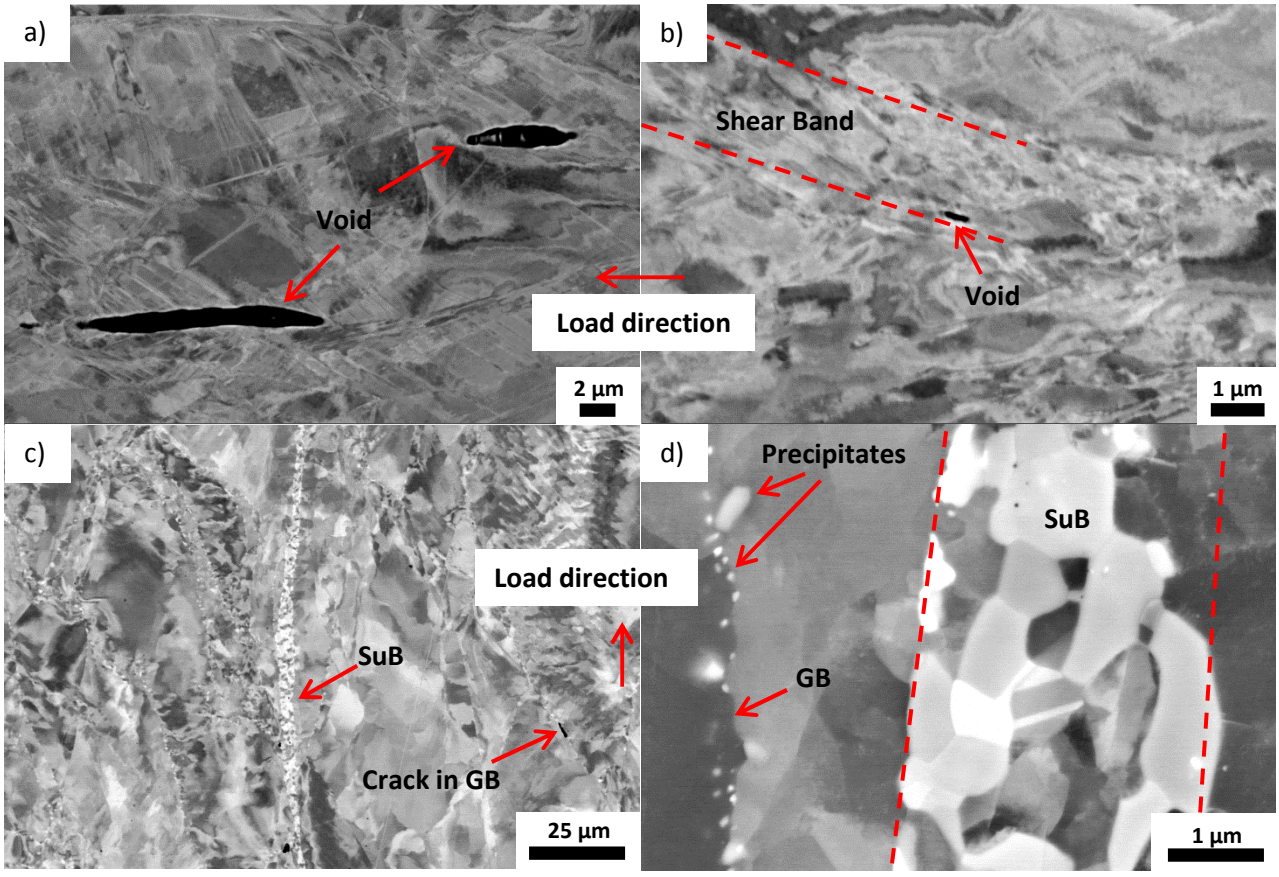

Figure 4. Deformation and damage behavior by ECCI in AISI 316L materials, a) voids from interaction between slip bands and grain boundaries (GB) at RT and strain rate $2*10^{-3}$/s, b) void due to deformation from shear band at RT and 10^{-6}/s, c) subcell band (SuB) at 650°C and 10^{-6}/s and d) magnification of subcell band.

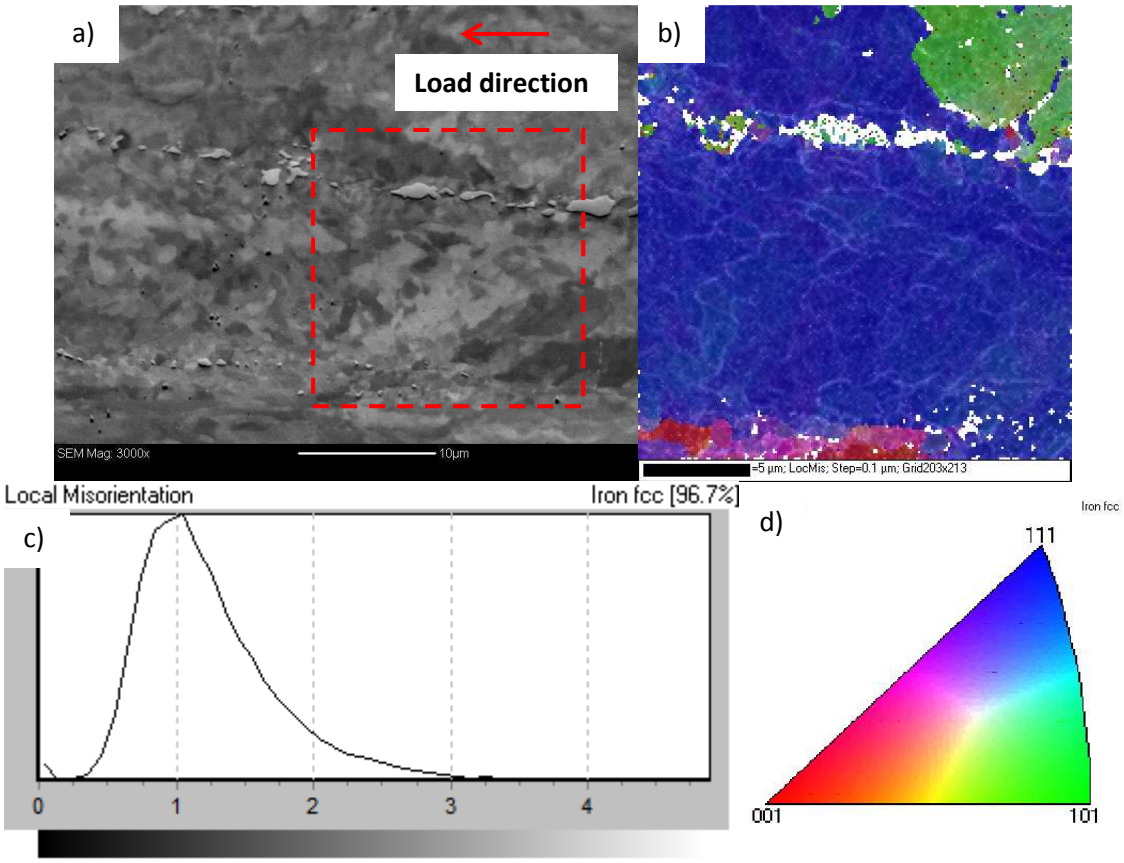

Figure 5. EBDS analysis showing recrystallization or subcell formation in AISI 316L after SSRT at 650°C to fractured using a strain rate of 10^{-6}/s, a) showing analyzed area, b) EBSD analysis displaying local misorientation (bright patterns) tighter with crystallographic orientation in a inversed pole figure (white color means zero-solution), c) local misorientation legend where the y-axis is frequency and x-axis is misorientation angle [°] and d) inversed pole figure legend showing crystallographic orientation.

3.2. Precipitates effect on damage

Both materials undergo precipitation due to the elevated temperature during the long deformation process. Alloy 617 has evenly distributed γ´ precipitates in the matrix and σ-phase in the grain boundaries [14]. AISI 316L get precipitates as Cr-rich carbides, that probably are $M_{23}C_6$ or M_6C, also σ-phase precipitate and they appear both in the matrix and grain boundaries [15]. The deformation time depends on material properties and strain rate, the deformation time varied from 1 minute to 130 hours. The size and amount of precipitates varied with the deformation time or strain rate and temperature, from no precipitate at high strain rates to more and bigger precipitates at the slower strain rates. Damage corresponding to the precipitation can be seen in fig.3 and fig. 6. At low strain rate and elevated temperature, the interaction between a moving dislocation and a precipitate can cause damage in the material. Fig. 6 display internal cracks that have initiate and propagate in the grain boundaries due to deformation and embrittlement from precipitates (Fig.6 c) and d)). Precipitates act as crack initiation points due to high local stress caused by the interaction between dislocations and precipitates.

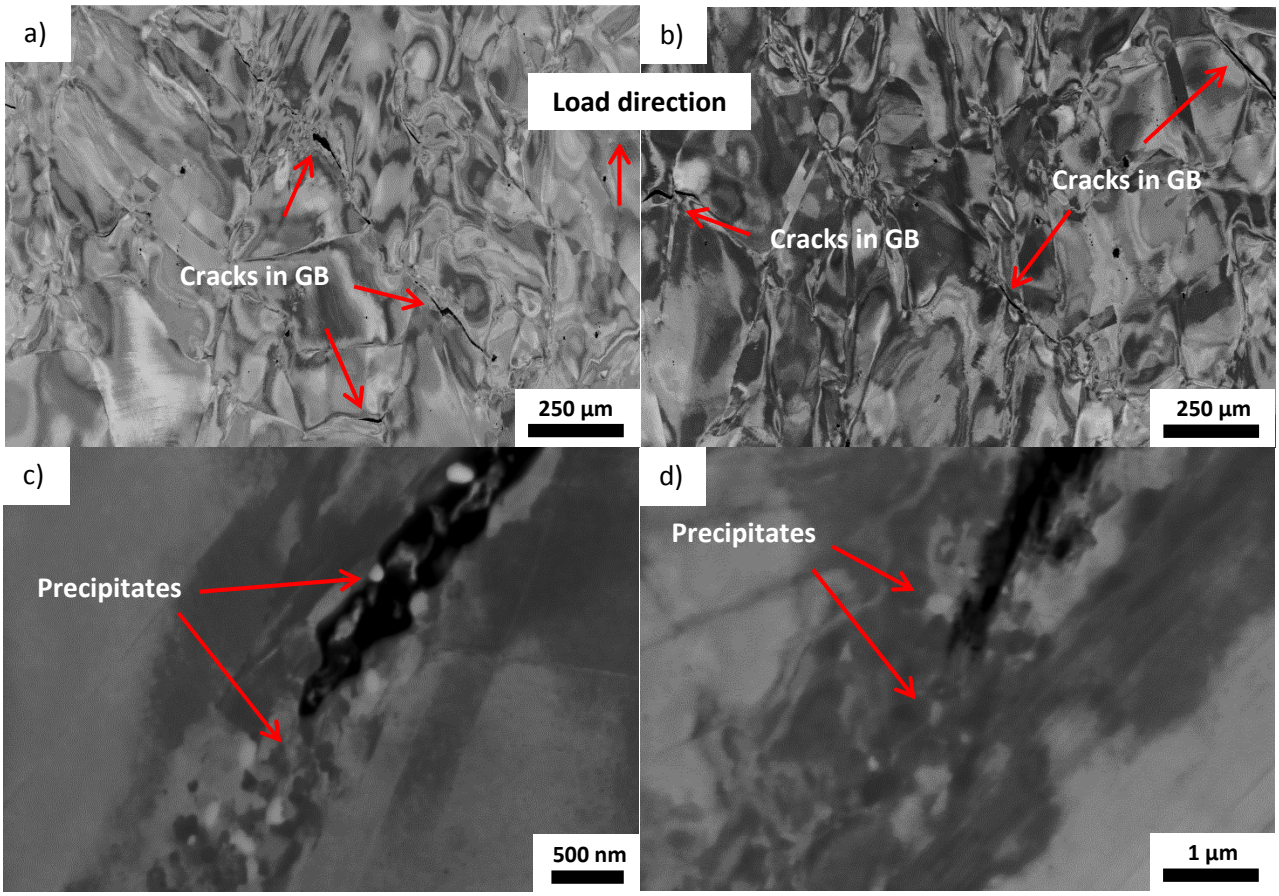

Figure 6. ECCI-picture showing internal cracks in the grain boundaries (GB) in Alloy 617, strain rate 10^{-5}/s and temperature a) 650°C, b) 700°C, c) crack tip, 650°C and b) crack tip, 700°C, tested to fracture. It is the same load direction in all the pictures.

4. Discussion

As known, DSA intensifies with increasing temperature and decreasing strain rate. However, in Alloy 617, DSA is present during the whole tensile deformation at elevated temperature when using a strain rate of 10^{-2}/s, but seems to disappear when the strain reach medium-high levels at an elevated temperature when using strain rates of 10^{-3}/s and 10^{-4}/s. DSA also appear again just before fracture when testing at elevated temperature using a strain rate of 10^{-3}/s. This behaviour could be described as a mismatch of the rates of solute atoms and moving dislocation, which could differ along the stress-strain curve and therefore serrations can appear just before fracture, where the local strain rate might be higher.

At room temperature the strain rate influencing the elongation in AISI 316L, when the strain rate decreases the elongation increases, also the stress level is lower at low strain rate. This is the result of the competition between hardening due to deformation and recovery due to the slow strain rate, where the recovery have more influence at slow strain rates than at higher. The recovery has a lager influence at lower deformations rates due to the fact that the moving dislocation rate decrease which affect the hardening to decrease. At high temperature the recovery probably can be an effect of creep, due to increasing diffusion rate and low deformation rate [11]. No clear microstructural signs as higher density of voids have been seen but they may be vanished due to high plastic deformation when the specimen is deformed to fracture. However, another sign that can be related to creep have been discovered, cell or subcell structure probably formed by creep deformation, from the EBSD-

analysis it is shown that the areas that look like recrystallization only have up to 5° misorientation which gives evidence for cell or subcell structures formed by creep deformation. According to the ECCI investigation there is areas and/or bands that display such cell or subcell structure, see fig.4c) and d). Further investigations are needed to confirm whether the cell or subcell structure is formed due to creep deformation in the AISI 316L material.

Elevated temperature and low strain rate decrease the ductility due to grain boundary embrittlement referred as sensitization and in some cases DSA. Sensitization is when chromium diffuses to the grain boundaries creating Cr-rich precipitates [16-19]. For sensitization the ageing time must be long enough for the precipitation to take place. According to literature sensitization occurs in AISI 316 material after less than 1h up to 100h depending on alloy content at 650°C and 700°C [17, 19]. After SSRT with a strain rate of 10^{-4}/s there are precipitates in the grain boundaries but they are too small to produce large scale embrittlement resulting in less internal cracks and larger elongation to fracture. For higher temperatures and long ageing times as in the case of SSRT tests with a strain rate of 10^{-6}/s and 700°C (fig.5 d)), desensitization probably can occur which means that chromium diffuses back into the interfacial region where the precipitate have grown [16, 19]. The desensitization seems to increase or keep the embrittlement of the material constant, see fig.2. In fig.2 b) the tensile stress increases which could refer to a hardening coupled to DSA that explain the large decrease in ductility. As known, precipitates in the matrix play two important roles for the life of the material, the first is to interact with moving dislocation and increase the strength or hardness of the material. The second is to cause stress concentration at the precipitate during dislocation accumulation that will in turn cause initiation of cracking by either precipitate cracking self or in the matrix.

5. Conclusion

After slow strain rate tensile testing at elevated temperatures and subsequent investigation of the microstructure using ECCI the following conclusions has been reached:

- Damage appears at interactions between moving dislocations and precipitates due to local stress concentration.

- DSA is present at all tested strain rates, but disappear at certain strain values for some deformation conditions. This is due to mismatches in the rates of moving dislocations and solute atoms at different strain intervals during the tensile deformation.

- Grain boundary embrittlement is causing damage as internal cracks and lowers the elongation to fracture. Therefore it is strongly affecting the material fracture behaviour at elevated temperature and is affecting for the high-temperature performances during deformation of the tested materials.

- AISI 316L show behaviour similar to creep at low strain rates (10^{-6}/s) and high temperatures.

Acknowledgements

Present study was financially supported by AB Sandvik Material Technology in Sweden and the Swedish National Energy Administration through the Research Consortium of Materials Technology for Thermal Energy Processes, Grant No. KME-501. Agora Materiae and Strategic Faculty Grant AFM at Linköping University are also acknowledged.

References

[1] J. Pettersson, H. Asteman, J. Svensson, L. Johansson, KCl Induced Corrosion of a 304-type Austenitic Stainless Steel at 600°C; The Role of Potassium, Oxidation of Metals. 64 (2005) 23-41.
[2] R. Viswanathan, K. Coleman, U. Rao, Materials for ultra-supercritical coal-fired power plant boilers, Int. J. Pressure Vessels Piping. 83 (2006) 778-783.
[3] L.H. de Almeida, I. Le May, P.R.O. Emygdio, Mechanistic Modeling of Dynamic Strain Aging in Austenitic Stainless Steels, Mater Charact. 41 (1998) 137-150.
[4] W. Karlsen, M. Ivanchenko, U. Ehrnstén, Y. Yagodzinskyy, H. Hänninen, Microstructural manifestation of dynamic strain aging in AISI 316 stainless steel, J. Nucl. Mater. 395 (2009) 156-161.
[5] M.A. Soare, W.A. Curtin, Solute strengthening of both mobile and forest dislocations: The origin of dynamic strain aging in fcc metals, Acta Materialia. 56 (2008) 4046-4061.
[6] A.W. Sleeswyk, Slow strain-hardening of ingot iron, Acta Metallurgica. 6 (1958) 598-603.
[7] S. Hong, S. Lee, Mechanism of dynamic strain aging and characterization of its effect on the low-cycle fatigue behavior in type 316L stainless steel, J. Nucl. Mater. 340 (2005) 307-314.
[8] K.G. Samuel, S.L. Mannan, P. Rodriguez, Serrated yielding in AISI 316 stainless steel, Acta Metallurgica. 36 (1988) 2323-2327.
[9] P. Rodriguez, Serrated plastic flow, Bulletin of Materials Science. 6 (1984) 653-663.
[10] I. Gutierrez-Urrutia, S. Zaefferer, D. Raabe, Electron channeling contrast imaging of twins and dislocations in twinning-induced plasticity steels under controlled diffraction conditions in a scanning electron microscope, Scr. Mater. 61 (2009) 737-740.
[11] R. Lagneborg, Recovery creep in materials hardened by a second phase, J. Mater. Sci. 3 (1968) 596-602.
[12] G.R. Stewart, A.M. Elwazri, S. Vue, J.J. Jonas, Modelling of dynamic recrystallisation kinetics in austenitic stainless and hypereutectoid steels, Materials Science and Technology. 22 (2006) 519-524.
[13] M. Calmunger, G. Chai, S. Johansson, J. Moverare, Influence of Dynamic Strain Ageing on Damage in Austenitic Stainless Steels, ECF19. (2012).
[14] M. Speicher, A. Klenk, K. Maile, E. Roos, Behaviour of Ni-based alloys for fossil-fired power plant components in the long-term creep regime, Advanced Materials Research. 278 (2011) 241-246.
[15] O.H. Ibrahim, I.S. Ibrahim, T.A.F. Khalifa, Effect of Aging on the Toughness of Austenitic and Duplex Stainless Steel Weldments, Journal of Materials Science & Technology. 26 (2010) 810-816.
[16] E.A. Trillo, R. Beltran, J.G. Maldonado, R.J. Romero, L.E. Murr, W.W. Fisher, A.H. Advani, Combined effects of deformation (strain and strain state), grain size, and carbon content on carbide precipitation and corrosion sensitization in 304 stainless steel, Mater Charact. 35 (1995) 99-112.
[17] S.K. Mannan, R.K. Dayal, M. Vijayalakshmi, N. Parvathavarthini, Influence of deformation on sensitization kinetics and its microstructural correlation in a nuclear grade 316 stainless steel, J. Nucl. Mater. 126 (1984) 1-8.
[18] N. Parvathavarthini, R.K. Dayal, Time–temperature-sensitization diagrams and critical cooling rates of different nitrogen containing austenitic stainless steels, J. Nucl. Mater. 399 (2010) 62-67.
[19] A.Y. Kina, V.M. Souza, S.S.M. Tavares, J.M. Pardal, J.A. Souza, Microstructure and intergranular corrosion resistance evaluation of AISI 304 steel for high temperature service, Mater Charact. 59 (2008) 651-655.